Self-organization mechanisms in a Fe-Au film: from isolated core-shell to multicore nanoparticles

Ségolène Combettes, Teresa Hungria, Sophie Barre, Béatrice Pecassou, Robin Cours, Magali Benoit, Marie-José Casanove, Anne Ponchet, Patrizio Benzo, Robin Recours

Eur. Phys. J. Appl. Phys. **97**, 27 (2022)

https://doi.org/10.1051/epjap/2022220026

Special Issue on 'Nanoalloys: Kinetic and Environmental Behaviour', edited by Pascal Andreazza, Riccardo Ferrando and Liu Xiaoxuan

THE EUROPEAN PHYSICAL JOURNAL APPLIED PHYSICS

Regular Article

Self-organization mechanisms in a Fe-Au film: from isolated core-shell to multicore nanoparticles

Ségolène Combettes[1], Teresa Hungria[2], Sophie Barre[1], Béatrice Pecassou[1], Robin Cours[1], Magali Benoit[1], Marie-José Casanove[1], Anne Ponchet[1], and Patrizio Benzo[1,*]

[1] CEMES, CNRS UPR 8011 and Université de Toulouse, 29 rue Jeanne Marvig, F-31055 Toulouse, France
[2] Centre de MicroCaractérisation Raimond Castaing, Université de Toulouse, 3 rue Caroline Aigle, F-31400 Toulouse, France

Received: 3 February 2022 / Received in final form: 18 March 2022 / Accepted: 28 March 2022

Abstract. Many nanotechnological applications necessitate a high density of nanoparticles (NPs), making NP morphology control highly challenging. In this work, the morphology of bimetallic NPs formed by magnetron sputtering deposition of a Fe(3 nm)-Au(2 nm) bilayer film on an amorphous silica substrate is analyzed using high-angle dark-field scanning transmission electron microscopy (HAADF-STEM). While all the NPs adopt a Fe-Au core-shell chemical order, they can be sorted into three different types. Isolated NPs, displaying either a highly symmetric centered core geometry (CC-type) or an asymmetrical off-centered core geometry (OC-type), are observed despite the rather large metallic volume. The majority of the NPs however displays a multicore geometry, with Fe cores in the 10-12 nm range, larger than the NPs observed in a pure Fe (3 nm) film grown under identical conditions. The driving forces leading to the different morphologies are discussed together with the role played by the environnement.

1 Introduction

Metal nanostructures are the building blocks of a wide range of applications in the fields of biosensing, plasmonics, magnetism, magneto-optics or catalysis [1–6]. The formation of self-organized films of metal nanoparticles (NPs) has therefore been extensively studied, including the exploration of new routes such as pulsed laser melting [7,8] or solid state dewetting [9–11]. Among the metal nanostructures of interest, those combining different metals are most appropriate for designing multifunctional materials, in particular when the two metals present large miscibility gaps. In this context, nanostructured films combining a ferromagnetic metal and a noble metal, distributed in well-separated nanoscale domains, have received considerable attention and have been developed in various systems such as Ni-Ag [12], Co-Ag [8], Fe-Ag [13] and Fe-Au [9] (or FeRh-Au [14]). The size, shape, and spatial organization of the nanostructures, as well as the distribution of the different metals in the multicomponent nanostructures, will directly influence the properties. It is therefore essential to control these features, and in particular to gain deeper understanding of the mechanisms giving rise to a particular organization.

In this paper, we focus on the Fe-Au system. Thanks to their low miscibility at room temperature [15], Au and Fe are distributed in two well separated phases, preserving their own properties. Previously, we succeeded in growing assemblies of well-faceted Fe@Au (core@shell) nanocrystals by magnetron sputtering [16], and gave evidence of the role of the shell thickness in their morphology [17]. More precisely, for low shell/core volume ratios, a polyhedral shape is adopted both for the core (iron) and the shell (gold), while, when this ratio is greater than 1, the Fe core adopts a quasi-cube shape and is surrounded by 6 truncated Au square pyramids forming the shell. We demonstrated that these different morphologies correspond to equilibrium shapes resulting from the combination of three driving forces: wetting, gold surface energy minimization, and Au/Fe interface energy minimization [18,19]. These driving forces come from three characteristics of the Au-Fe system: (i) the high ability of Au to completely wet Fe nanocrystals, thanks to the large difference in their surface energies, 1.500 J.m^{-2} for (111) Au compared to 2.417 J.m^{-2} for (110) Fe (experimental values) [20]; (ii) the difference in the Fe and Au crystal structures, respectively the body-centered cubic (bcc) structure for Fe and the face-centered cubic (fcc) structure for Au; (iii) the existence of two preferred Au/Fe interfaces respectively coherent and semi-coherent, that determines the effective interfacial misfit. The coherent interface, schematized in Figure 1a is parallel to the {100} crystal plane family in both Fe and Au crystal lattices, Au growing over the Fe lattice according to the Bain epitaxial relationship:

$$Au\,\{100\}\,\langle 100\rangle\,//\,Fe\,\{100\}\,\langle 110\rangle\,.$$

This interface, hereafter referred as P_B, presents a lattice misfit as low as 0.6%. The semi-coherent interface, shown in Figure 1b, is parallel to the highest-density

* e-mail: benzo@cemes.fr

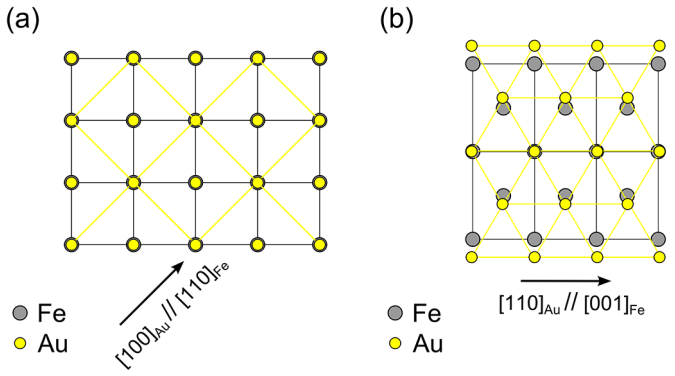

Fig. 1. Epitaxial relationships of the P_B (a) and P_{NW} (b) interfaces observed in plan view.

planes in both structures, i.e the {111} in the fcc lattice and the {110} in the bcc one. In the Fe-Au system, the epitaxial relationship expected at this interface [21] is the Nishiyama-Wasserman (NW) relationship:

$$Au\,\{111\}\,\langle 110\rangle\,//Fe\,\{110\}\,\langle 100\rangle\,.$$

As observed in the figure, this interface, referred as P_{NW}, is highly misfitted along the $\langle 110\rangle_{Fe}$ direction in the $\{110\}_{Fe}$ plane. Clearly, the P_B and P_{NW} interfaces compete in the core@shell geometry [18,19].

The core-shell geometry is particularly interesting for applications as the chemically inert Au shell provides oxidation protection for the ferromagnetic iron core and additionally offers a unique platform for biosensing or bioconjugation. This geometry also proves very robust and was obtained by different authors using various growth conditions and methods [9,22–24].

However, for most applications, it is desirable to increase the density of the NPs in order to improve the device's response without increasing its size. An important drawback of higher density is that the intrinsic properties of each NP may be lost or weakened as a result of its interactions with surrounding NPs (see for instance, Hillion et al. [25] for magnetic interactions). Increasing the NPs density also raises several morphological issues. Is the geometry of small isolated NPs preserved when their density increases ? Is it possible to achieve a large density of small NPs, or does the deposit evolve towards a low density of large NPs ? To address these questions, in the present paper, we analyze the structural behavior of films including a much larger quantity of Fe than in our previous studies of this system [16–19], in view of increasing the NPs density or size. Pure Fe and Au capped Fe (Fe-Au) films, deposited at a temperature favoring the 3D growth of both metals, are compared. We highlight the abrupt evolution of the iron layer and self-organization in the Fe-Au film compared to the pure Fe film. The respective role of surface and interface properties and mobility in the observed nanostructures is discussed.

2 Experimental details

The FeAu films were grown on amorphous silica (SiO_2) by dc magnetron sputtering from two high purity Fe and Au elemental targets in an ultra-high vacuum (UHV) chamber. In order to facilitate transmission electron microscopy (TEM) expriments, the silica buffer layer, about 5 nm thick, was itself deposited on a water soluble NaCl crystal. The Fe and Au layers were sequentially deposited at a same temperature of 600°C with a growth rate of 0.017 nm/s and 0.033 nm/s respectively. The nominal deposited thicknesses were $t_{Fe} = 3$ nm for the iron layer and $t_{Au} = 2$ nm for the gold layer. Finally a 5 nm thick amorphous silica cover layer was deposited at room temperature to prevent water damage during the removal of the NaCl support. We previously verified that this cover layer was effective against iron oxidation and did not change the morphology of the metallic film [17]. The Au layer deposition step was skipped in one of the samples in order to analyze the 3 nm Fe film before the deposition of the Au layer. This sample will be further referred as Fe_3Au_0 while the bimetallic sample will be referred as Fe_3Au_2.

Plan-view specimens were prepared for transmission electron microscopy (TEM) experiments by transferring the SiO_2 films containing the metallic layers onto TEM copper grids, after dissolution of the NaCl substrate in deionized water. A cross-sectional lamella was also prepared by Focused Ion Beam (FIB) in a ThermoFisher Helios Nanolab 600i. The sample surface was protected by a 1.5 μm thick Pt layer to avoid damages during the thinning process. The lamella was then extracted and thinned down to less than 100 nm to get electron transparency with a final step at low energy to minimize irradiation damages. Atomically resolved high-angle annular-dark-field scanning TEM (HAADF-STEM) experiments were conducted using a probe corrected JEOL ARM200F microscope.

3 Results

3.1 Comparison between pure and Au capped Fe nanoparticle films

The comparison of a pure Fe film with a film grown under the same conditions but capped with a Au layer allows us to better understand the stages of transformation induced by the Au capping. Figure 2 presents HAADF-STEM images of plan view specimens corresponding to the two samples, Fe_3Au_0 (Fig. 2a) and Fe_3Au_2 (Fig. 2b). Clearly, both samples consist in assemblies of nanoparticles, a Volmer-Weber (3D) growth mode on silica being favored by this growth temperature.

Figure 2a exhibits a high density of Fe nanoparticles, imaged in bright contrast on the SiO_2 substrate. These NPs are rounded or slightly elongated. Besides, they are crystalline as seen in the inset of Figure 2a. Their size distribution is relatively narrow with a standard deviation 2.2 nm around the mean diameter 7.8 nm. Please note that in the case of elongated NPs, the longest axis was measured.

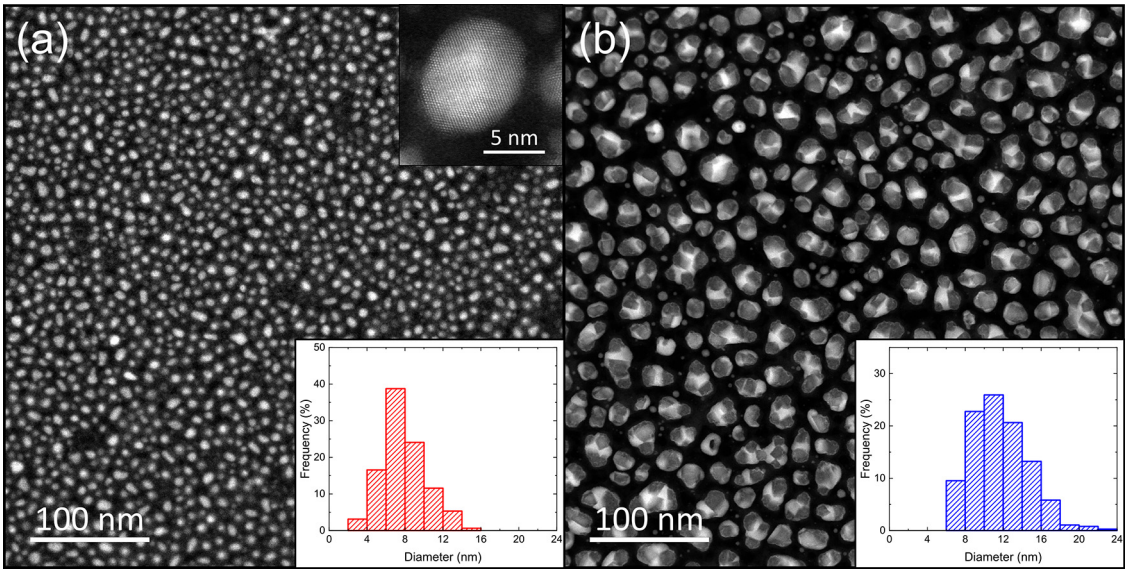

Fig. 2. HAADF-STEM plan view images of Fe_3Au_0(a) and Fe_3Au_2(b) samples showing the drastic morphological transformation of the Fe thin film when covered by a thin Au layer. A high-resolution HAADF-STEM image of a typical Fe NP is displayed in inset at the top of Figure (a). Note that, owing to the sensitivity of HAADF-STEM images to the atomic number of the compounds, the Fe NPs exhibit a bright contrast in (a) but a grey contrast in (b), the bright contrast being displayed by Au. The darker regions correspond to the silica matrix in both images. Bottom insets show the size histograms of the Fe NPs (Fig. a) and the Fe cores (Fig. b).

Table 1. Size distribution (mean diameter $\langle d \rangle$ and standard deviation σ) and density of the Fe NPs (uncapped Fe films) or Fe cores (Au-capped Fe films).

Sample	$\langle d \rangle$ (nm)	σ (nm)	Density (Fe) (NPs/cm^2)
Fe_3Au_0	7.8	2.2	8.42x10^{11}
Fe_3Au_2	11.6	2.9	2.90x10^{11}

The image of sample Fe_3Au_2 reveals a drastic decrease of the NPs density (Fig. 2b). A close observation of the NPs provides evidence for the presence of two different phases. Owing to the sensitivity of the HAADF-STEM imaging mode to the atomic number of the elements, the brighter contrast can now be attributed to the Au phase, while the Fe phase is imaged in a dark grey contrast, lighter than the SiO_2 substrate.

The size distribution and density of Fe NPs (in Fe_3Au_0) and Fe cores (in Fe_3Au_2), recorded from image analyses, are reported in Table 1. Remarkably, the density of Fe cores after gold capping is about 3 times lower than the initial density of NPs in Fe_3Au_0. In parallel, Fe cores in Fe_3Au_2 have a larger mean size $\langle d \rangle$ than the mean diameter of Fe NPs in sample Fe_3Au_0.

3.2 Evidence of different geometries in the Fe_3Au_2 film

All nanoparticles in the FeAu film display a bright contrast at their surface in HAADF-STEM images (Fig. 3), which reveals the presence of a Au shell. However, they

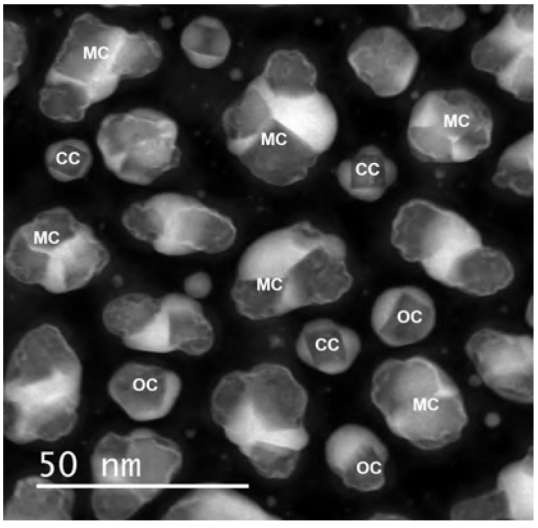

Fig. 3. HAADF-STEM plan view image of the Fe_3Au_2 sample showing the different geometries. Labels CC, OC or MC have been added on some easily identified geometries.

display various geometries which can be classified in three types: i) small Fe@Au core-shell NPs (6-10 nm large) displaying a centered core with cubic shape surrounded by a well-faceted Au shell (referred as CC for centered core); ii) NPs, in the 16-22 nm range, displaying an off-centered core (referred as OC for off-centered core). iii) much larger NPs formed of two or more different Fe cores embedded in a gold matrix (referred as MC for multicore NPs).

Note that, the formation of MC nanoparticles induces a lower bimetallic NP density in sample Fe_3Au_2 (1.43x10^{11}

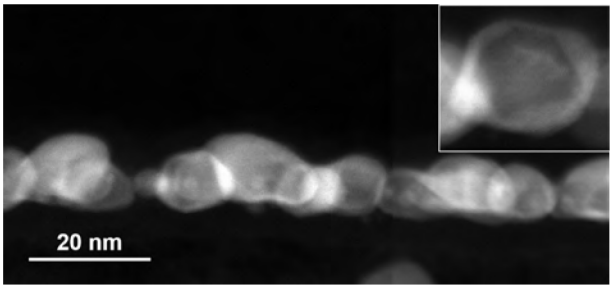

Fig. 4. Cross-sectional view of the Fe_3Au_2 sample observed in HAADF-STEM mode. A centered-core NP is displayed at higher magnification in the inset.

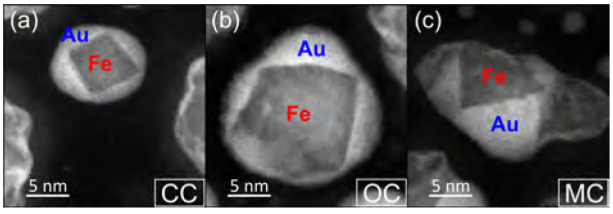

Fig. 5. Atomically resolved HAADF-STEM images of the three types of geometry observed in Fe_3Au_2 sample.

NPs/cm^2) than the Fe core density in the same sample, reported in Table 1.

To get a better insight on the 3D morphology of the NPs, a HAADF-STEM image of the cross-sectional specimen is presented in Figure 4. In this kind of view, it is more difficult to distinguish all the different NPs, as NPs are much smaller than the FIB lamella thickness and thus appear superimposed in the image. Nevertheless, this view provides clear evidence for the presence of a Au shell fully embedding the different NPs and in particular at the bottom interface with SiO_2. The thickness of the NPs in the growth direction typically ranges between 8 and 12 nm and never exceeds 12 nm in the cross-sectional observations.

The structural features of these different geometries are better observed in Figure 5 and will be described below. A common feature in the different types of NPs is their high crystallinity. The iron cores mainly form single crystals while the Au shell is polycrystalline, as we previously observed [16–18]. Indeed, due to the epitaxial relationships (cf. Fig. 1), each Fe core facet generates a particular orientation of the Au shell.

3.2.1 Centered core NPs

The CC type represents about 15% of the observed NPs. They are 6-12 nm large, well isolated on the substrate and present the smaller Fe cores. As illustration, the CC NPs seen in Figure 3 have a core width from 6.4 to 9.8 nm (average 8.2 nm), well corresponding to the initial core size reported in Table 1 for the Fe_3Au_0 sample. The cores adopt a quasi-cube shape surrounded by six ⟨001⟩ oriented truncated Au pyramids, forming a polycrystalline shell (each pyramid is one single-crystal). Most of the interfaces observed edge-on are large, flat and parallel to a crystal plane; they are clearly identified of the P_B

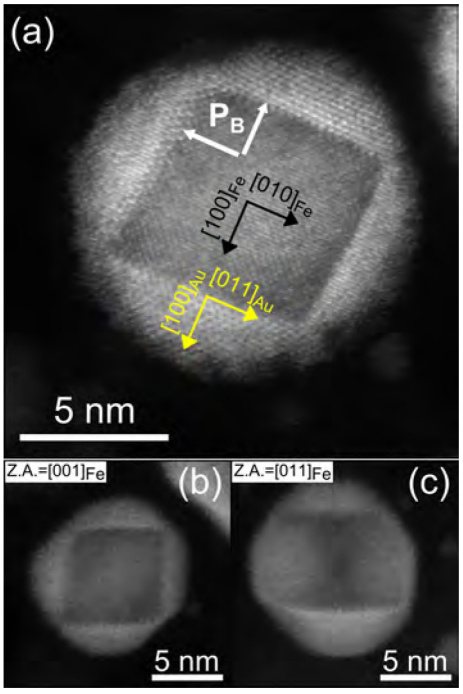

Fig. 6. Plan view observation of CC NPs. a) Atomically resolved HAADF-STEM image of a CC NP showing four neat P_B Au/Fe interfaces. b) CC NP observed along a $[001]_{Fe}$ zone axis; c) CC NP observed along a $[011]_{Fe}$ zone axis.

type, as observed in Figure 6a, with eventually short P_{NW} segments at the cube edges. Most of the CC NPs are oriented with one ⟨001⟩ direction of the core normal to the substrate, as in Figure 6a and Figure 6b, so that four interfaces are seen edge-on in plan-view and four pyramids are well observed. Some CC NPs have nevertheless adopted another orientation, as in Figure 6c, with a ⟨011⟩ direction of the core normal to the substrate (only two interfaces are edge-on). Note that the cube shape and the pyramids are well observed also in cross-section (inset of Fig. 4).

3.2.2 Off-centered core NPs

Off-centered NPs (about 25%) have a core in the 8-16 nm range and up to 20 nm, much larger than the Fe NPs size in the Fe_3Au_0 sample. They display a highly asymmetrical geometry (Fig. 7). Indeed, the Fe core is coated on one side by a few Au monolayers (outer boundaries), while large Au grains grow on the other side (inner boundaries) . This asymmetrical morphology gives rise to various Au/Fe interfaces. Large P_B type interfaces preferentially form at the inner boundaries and are topped by large truncated Au pyramids, as in CC NPs. At the outer boundaries, one can find either P_{NW} Au/Fe flat interfaces or stepped interfaces, referred as S-type in Figure 7. These interfaces are covered by a thin Au wetting layer. The S-type interface seems mainly composed of short segments parallel to $\{100\}_{Fe}$ plane family. The different kinds of interface are observed edge-on in Figure 7. The presence of a grain boundary at the junction between the Au grains grown over two Fe ⟨100⟩ facets forming a right angle, is

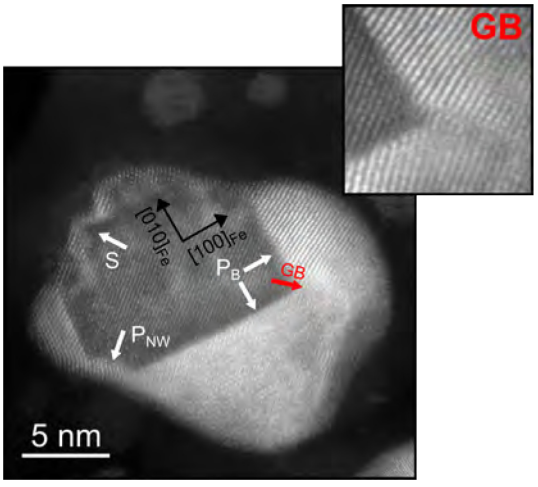

Fig. 7. Atomically resolved HAADF-STEM image of an OC type nanoparticle observed in plan-view along a $\langle 100 \rangle_{Fe}$ axis. P_B Au/Fe interfaces are clearly identified at the inner boundaries in the NP, while P_{NW} and stepped, S, Au/Fe interfaces are found at the outer boundaries. Inset: enlarged view of the grain boundary (GB) formed at the junction between the two Au grains grown over the core cube facets (P_B interfaces), owing to their different orientations. Note the presence of dislocations at this GB.

indicated by a red arrow in the figure. A high resolution image of this grain boundary is shown in the inset.

3.2.3 Multicore NPs

The large majority of the observed NPs are formed of two or more Fe cores (up to 6) fully embedded in a gold matrix and are thus referred as multicore NPs (about 60%) (see for instance Fig. 3). The mean diameter, 11.6 nm, reported in Table 1, thus essentially reflects the size of the Fe cores in MC NPs. As can be observed in Figure 3 and Figure 5c for instance, most of the cores adopt an asymmetrical shape. At their inner boundaries, the cores are bounded by polygonal facets, including P_B and P_{NW} interfaces. The P_B type interfaces are often observed edge-on and thus clearly identified. At their outer boundaries, the cores are coated by a polycrystalline Au wetting layer, with a thickness not exceeding a few monolayers. As in the OC NPs, the outer interfaces are essentially stepped, but can also include narrow P_{NW} facets. A single core in MC NPs thus roughly displays the same features as the off-centered core in OC NPs. Remarkably, the different cores of a same MC NP essentially lie at its outer side and are separated by large Au grains. They can have the same orientation and be aligned, however misaligned cores with different orientations are the most common.

4 Discussion

4.1 Adhesion and orientation of the NPs on silica

First we will discuss the role of the substrate in the NPs formation. Initially, the Fe nanocrystals are in a Volmer-Weber (i.e. partial wetting) equilibrium state on the silica substrate as in the Fe_3Au_0 sample. After Au deposition, they are completely replaced by core-shell NPs, also in a Volmer-Weber equilibrium state on silica. A striking feature revealed by cross-sectional observations is that Au has diffused at the bottom Fe/silica interface so that the Fe nanocrystals are fully embedded by Au. This indicates that replacing the single Fe/SiO_2 interface by two interfaces, Au/SiO_2 and Au/Fe, is energetically favorable.

According to the Au-Fe phase diagram [15], the bulk diffusion of Au into the Fe bcc phase is still very small at the chosen deposition temperature. The diffusion of Au at interfaces should thus be the most active mechanism of diffusion and is also favored because the Fe NPs and the amorphous silica form an incoherent interface with a low contact area. Au diffusion was also recently reported at a metal-ceramic interface, namely the Ni-sapphire interface [26]. The authors demonstrate that this interface diffusion was faster than the bulk diffusion of Au in Ni, in the investigated range of annealing temperature (450-550°C). In addition, remarkably, not only Au diffuses at the Fe/SiO_2 interface, but it can also form faceted pyramids at the bottom of the Fe core. As observed in the inset of Figure 4, the pyramid at the interface with SiO_2 has nearly the same shape and size as the pyramids grown at the free surface of this CC NP. Moreover, this NP displays the cubic symmetry expected for a fully free Fe@Au NP at equilibrium. [18,19] Thus, the shape of the Fe@Au NPs seems to be only very slightly affected by the interfaces with silica. This indicates that the adhesion energy of the observed Fe@Au NPs on silica, although non-null, is particularly weak. From this point of view, Fe@Au NPs on silica behave as pure Au droplets, which exhibit a small adhesion on silica, as experimentally attested (work of adhesion around 310-360 $mJ.m^{-2}$) [27,28]. This weak adhesion thus explains the high mobility of Au on silica.

Clearly, the amorphous silica substrate favors the evolution toward the fully embedded core@shell morphology, and could also have a role in the two preferential orientations of the NPs. Indeed, preferential (100) and (111) orientations of the metal are reported for interfaces between fcc metals and silica, at the growth temperature of our experiments [29]. It turns out that the NPs have most frequently one $\langle 001 \rangle_{Fe}$ direction close to the normal to the substrate (as in Fig. 6b), and thus should have a $(100)_{Au}$/silica interface. Other NPs are orientated with one $\langle 110 \rangle_{Fe}$ direction normal to the substrate (as in Fig. 6c) and their interface with silica is thus close to a $(111)_{Au}$/silica interface.

4.2 Formation mechanisms

Let us now consider the different types of NPs observed in the Fe_3Au_2 sample. The easiest case is the CC type as its morphology is similar to that previously reported for highly dispersed Fe core-Au shell NPs. [17]. According to an analytical model [18], this morphology corresponds to the equilibrium shape of an isolated core-shell NP when the gold/iron volume ratio is greater than 1. This observation suggests the occurrence of fluctuations of the Au/Fe volume ratio at the nanoparticle level, the nominal

deposited Au/Fe ratio being smaller than 1. The shape predicted by the model is displayed in Figure 8a with an Au/Fe volume ratio of 1.2 and a core volume of 475 nm^3 (i.e. a 7.8 nm cube edge). The quasi-cube shape is favored by the minimization of interface energy, the P_B type being far less expensive than the P_{NW} one, and the truncated pyramids are thus the optimal shape for minimizing the Au surface energy. Note that a growth simulation utilizing semi-empirical potentials produced the same shape [19].

In the present experiment, the core size of the CC NPs clearly indicates that they originate from the initial distribution of bare Fe nanocrystals.

Except for the CCs, all the NPs display much larger iron cores. While each CC-type NP is formed by the embedding of a single isolated initial Fe core with no contact with its neighbors, the large cores of the OC and MC NPs clearly result from a core coalescence process, in agreement with the difference in densities of Fe NPs (in sample Fe_3Au_0) and Fe cores in sample Fe_3Au_2. The coalescence is here favored by the high density of Fe NPs, the deposited volume being much higher than in previous studies of this system [16,17]. Our experiments do not allow us to draw any conclusions about the coalescence mechanism, particularly the role of Au in the coalescence of the Fe cores. Nevertheless, coalescence of the Fe NPs is unambiguously promoted by the deposition of the Au layer, as observed in Figure 2. This suggests that Au favors the mobility of the Fe cores, thanks to the very low adhesion energy of Au on silica conjugated to the easy formation of the Au wetting layer between the Fe core and the silica, as described in the previous section. Note that the smaller Fe NPs may also dissolve into the larger ones according to an Ostwald ripening mechanism, the diffusion of Fe atoms into Au being favored by the temperature (cf. Au-Fe phase diagram [15]).

In any case, the driving force for core coalescence is the minimization of the excess interface energy, thanks to the reduction of the interface area. Indeed, when a given volume V is distributed in a single core rather than in n identical cores of similar shape, one can easily demonstrate that the relative reduction of interface area due to a pure scaling effect is $n^{-1/3} - 1$. Note that this factor does not depend on the chosen core shape. The gain in excess interface energy is identical to the reduction in interface area if the shape does not evolve. Considering an average experimental $n = 3$, a rough estimation of the relative decrease of excess interface energy is -30% according to the above formula.

The large majority of the observed NPs display the MC type. MC NPs result from the conjugation of the coalescence of several Fe cores and of the coalescence of core-shell NPs in formation. As they grow, large cores formed by the coalescence of several initial Fe nanocrystals become progressively less mobile. Once fully embedded by gold, the core coalescence becomes extremely unlikely because the wetting by gold is the first driving force in this system. The shell coalescence however remains possible if several shells come in contact, or the Au atoms are sufficiently mobile on the surface. The coalescence of NPs already with a core-shell morphology results thus in the formation of large NPs of the MC type.

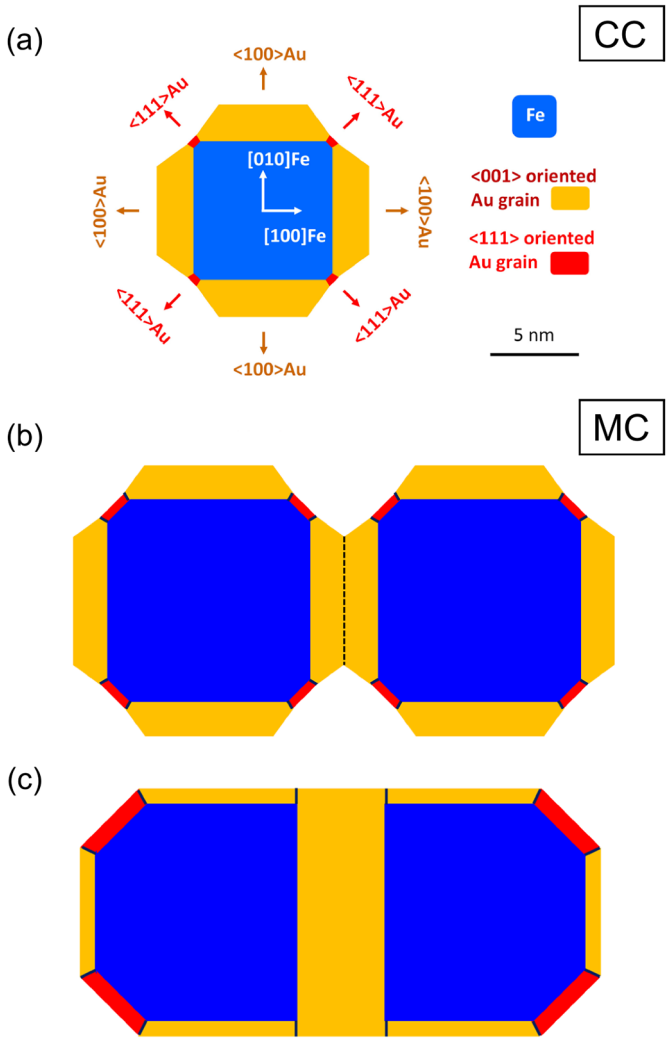

Fig. 8. (a) Equilibrium shape of an isolated CC Fe@Au NP with an Au/Fe volume ratio of 1.2 and a core volume of 475 nm^3 from an analytical model [18]. (b) Two identical CC NPs connected by their pyramids, each NP displaying the equilibrium shape of an isolated Fe@Au NP with an Au/Fe volume ratio of 0.67 and a Fe volume 1400 nm^3 from the analytical model. (c) A possible MC morphology using the same metallic volumes as in (b). Note that the density functional theory was used to compute the surface and interface energy in the analytical models of isolated CC NPs. The NP models are displayed in cross-sections.

The shapes are not preserved in this process. The final morphology of the MCs combines different elements that can be explained by energetic considerations:

(i) the gold shell tends to incorporate the various cores in a highly compact manner to reduce surface area and thus surface energy. For this, a large amount of Au fills the space between the cores.
(ii) The outer sides of the cores are only covered by a thin Au layer, which is required to ensure complete wetting.
(iii) The inner interfaces are planar (P_B type) and
(iv) the interface adopts a polyhedron shape at the outer

sides with small P_B and either P_{NW} or S interfaces.

To explain points (iii) and (iv), and in particular why the cores are no more symmetrical, it is interesting to compare the same volumes distributed in either an MC NP with two large cores or two identical CC NPs.

Figure 8b represents two identical single core CC NPs connected by their pyramids, each of these NPs being in the equilibrium shape it should adopt as long as it is isolated (N.B. the model ignores the interaction with silica), from reference [18]. The illustration is scaled for a core of 1400 nm^3 (i.e. 3 times larger than the core volume in Fig. 8a) with an Au/Fe volume ratio of 0.67. The core is a polyhedron, and the shell is composed of a few monolayers thick ⟨111⟩ oriented grains and flat pyramidal ⟨001⟩ oriented grains, grown on the P_{NW} and P_B interfaces, respectively. This morphology minimises the excess surface and interface energy and reduces the disorder due to Au grain boundaries. The excess surface and interface energy, determined using DFT calculated data [18], is 1.05 10^{-15} J. The connected configuration is more stable than two separated NPs thanks to the suppression of some of the Au surfaces. The excess energy is 2.02 10^{-15} J, providing an energy reduction of –4.4%. Note that the two connected pyramids now form a single grain.

Figure 8c displays a more compact morphology that intends to reproduce the observed (i) to (iv) features (the volumes being conserved). The compactness is due to the depletion of the shell to the benefit of the central zone. This, however, necessitates reorganizing the interfaces. In the central region, changing the interfaces from polyhedral (a mix of P_B and P_{NW} interfaces) to planar (P_B) not only allows for the gain of interface energy (the P_B interface being the most favorable), but also contributes to the reduction of the polycrystalline shell disorder. Indeed, a unique ⟨001⟩ oriented grain can then fill the gap between the two cores and the Au grain boundaries extension is minimized. On the contrary, at the outer sides, a more "rounded" polyhedron alternating P_B and P_{NW} interfaces is the optimal shape that preserves the complete wetting, as it was experimentally observed [17] and theoretically predicted [18] in isolated NPs when the available Au amount is very limited. The MC nanostructure displayed as illustration in Figure 8c has an excess surface and interface energy of 1.97 10^{-15} J, i.e. a reduction of -6.3% compared to the two isolated NPs. Moreover, the decreasing of the grain boundaries extension will provide an additional reduction of excess energy, not taken into account in the model.

Obviously, the cores in the experimental samples are not as well aligned and oriented as in this ideal representation, and the interfaces at the outer sides can be less regular (S-type sometimes replacing P_{NW} type). However, this model can explain which driving forces lead to the observed morphology of the MC NPs. One can conclude that the final shapes of the MC types NPs are close to the most stable for the amount of gold available, and given that core mobility has now been blocked.

As in MC NPs, the size of the cores in OC NPs shows that they result from the coalescence of several initial Fe nanocrystals. Although the NPs with one single large core retain some elements identified in the equilibrium shape of the small CC NPs, none of them retains a symmetrical shape. This indicates that the fusion of several cores cannot lead to a symmetrical shape of the NP. The origin of the asymmetry is not yet fully understood. The nature of the different types of interface could play an important part, as their kinetics should be rather different. Indeed, the attachment of Fe atoms to an Fe core during the deposition of the Au layer, should preferentially take place at stepped or defected interfaces as S and P_{NW}, the formation of kinks at coherent planar interfaces as P_B implying a large energy cost. The former interfaces should then progress easily while the latter should mainly grow in a same plane, forming wider coherent facets. In parallel, the Au atoms, which are very mobile during this growth phase, should be attracted towards the coherent interface region, according to the model and driving forces described above and already discussed. The growth of Fe cores on one side and of the Au shell on the other (in OC NPs) or at the inner side (in MC NPs) may thus participate to the observed asymmetry. Interestingly, some MC NPs with an uneven shell appear to have visible traces of previous OC NPs. However, determining the path leading to the MC and OC types remains difficult.

5 Conclusion

In conclusion, the high-temperature (600°C) growth of both Fe and Fe-Au films on amorphous silica results in the formation of a dense assembly of crystalline nanoparticles. However, while the pure Fe film is composed of roughly rounded NPs with a diameter about 8 nm, the Fe-Au film contains three types of geometry, all of which exhibit a core-shell chemical order, namely centered core (CC), off-centered core (OC), and multicore (MC) nanoparticles, with the latter being far more numerous. We showed that the CC type results from the embedding of one isolated initial Fe core, i.e.formed before the Au coverage, without any interaction with the neighboring NPs whereas both OC and MC NPs incorporate Fe cores (a single core for OC and up to 6 different cores for MC) with a larger size, around 11.6 nm, resulting from the coalescence of several initial Fe cores. From a combined experimental and analytical analysis, we showed that the driving forces in MCs include, as for CC NPs, the preservation of at least a thin wetting layer and an optimization of both interface and surface energy. This strongly suggest that, although rather different than the equilibrium morphology displayed by isolated Fe-Au CC NPs, the observed MC type becomes the stable morphology with increasing NP density. Interestingly, this Fe-Au film displays a self-organized nanostructure, which features (i.e. crystallinity, well isolated Fe cores with narrow size distribution embedded in an Au matrix, preferred structural orientations) are most suitable for both fundamental studies and technological applications.

This study was supported by the French National Research Agency (ANR) in the framework of its "Investissements d'Avenir" program, ANR-10-LABX-0037-NEXT.

Author contribution statement

All the authors were involved in the preparation of the manuscript. All the authors have read and approved the final manuscript.

References

1. Q. Fu, K.M. Wong, Y. Zhou, M. Wu, Y. Lei, RSC Adv. **5**, 6172 (2015)
2. C.M. Müller, F.C.F. Mornaghini, R. Spolenak, Nanotechnology **19**, 485306 (2008)
3. R. Sachan, S. Yadavali, N. Shirato, H. Krishna, V. Ramos, G. Duscher, S.J. Pennycook, A.K. Gangopadhyay, H. Garcia, R. Kalyanaraman, Nanotechnology **23**, 275604 (2012)
4. Y.J. Oh, J.H. Kim, C.V. Thompson, C.A. Ross, Nanoscale **5**, 401 (2013)
5. B. Zhang, M. Kalaswad, B.X. Rutherford, S. Misra, Z. He, H. Wang, Z. Qi, A.E. Wissel, X. Xu, H. Wang, ACS Appl. Mater. Interfaces **12**, 51827 (2020)
6. L. Armelao, D. Barreca, G. Bottaro, A. Gasparotto, S. Gross, C. Maragno, E. Tondello, Coord.Chem. Rev. **250**, 1294 (2006)
7. S.J. Henley, J.D. Carey, S.R.P. Silva, Phys. Rev. B **72**, 195408 (2005)
8. H. Krishna, N. Shirato, S. Yadavali, R. Sachan, J. Strader, R. Kalyanaraman, ACS Nano **5**, 470 (2011)
9. D. Amram, E. Rabkin, ACS Nano **8**, 10687 (2014)
10. A. Herz, D. Wang, T. Kups, P. Schaaf, J. Appl. Phys. **116**, 044307 (2014)
11. A. Herz, A. Franz, F. Theska, M. Hentschel, T. Kups, D. Wang, P. Schaaf, AIP Adv. **6**, 035109 (2016)
12. J. Petersen, S.G. Mayr, J. of Appl. Phys. **103**, 023520 (2008)
13. C. Binns, M.J. Maher, Q.A. Pankhurst, D. Kechrakos, K.N. Trohidou, Phys. Rev. B **66**, 184413 (2002)
14. P. Benzo, S. Combettes, C. Garcia, T. Hungria, B. Pécassou, M.J. Casanove, Cryst. Growth Des. **20**, 4144 (2020)
15. H. Okamoto, T. Massalski, L. Swartzendruber, P. Beck, Bull. Alloy Phase Diagr. **5**, 592 (1984)
16. C. Langlois, P. Benzo, R. Arenal, M. Benoit, J. Nicolai, N. Combe, A. Ponchet, M.J. Casanove, Nano Lett. **15**, 5075 (2015)
17. P. Benzo, S. Combettes, B. Pecassou, N. Combe, M. Benoit, M. Respaud, M.J. Casanove, Phys. Rev. Mater. **3**, 096001 (2019)
18. A. Ponchet, S. Combettes, P. Benzo, N. Tarrat, M.J. Casanove, M. Benoit, J. Appl. Phys. **128**, 055307 (2020)
19. S. Combettes, J. Lam, P. Benzo, A. Ponchet, M.J. Casanove, F. Calvo, M. Benoit, Nanoscale **12**, 18079 (2020)
20. W. Tyson, W. Miller, Surf. Sci. **62**, 267 (1977)
21. E. Bauer, J.H. van der Merwe, Phys. Rev. B **33**, 3657 (1986)
22. P. Wagener, J. Jakobi, C. Rehbock, V.S.K. Chakravadhanula, C. Thede, U. Wiedwald, M. Bartsch, L. Kienle, S. Barcikowski, Sci. Rep. **6**, 23352 (2016)
23. M. Kamp, A. Tymoczko, U. Schürmann, J. Jakobi, C. Rehbock, K. Räzke, S. Barcikowski, L. Kienle, Cryst. Growth Des. **18**, 5434 (2018)
24. A. Tymoczko, M. Kamp, O. Prymak, C. Rehbock, J. Jakobi, U. Schürmann, L. Kienle, S. Barcikowski, Nanoscale **10**, 16434 (2018)
25. A. Hillion, A. Tamion, F. Tournus, C. Albin, V. Dupuis, Phys. Rev. B **95**, 134446 (2017)
26. H. Barda, E. Rabkin, Acta Mater. **186**, 242 (2020)
27. J.Y. Kwon, T.S. Yoon, K.B. Kim, S.H. Min, J. Appl. Phys. **93**, 3270 (2003)
28. F. Ruffino, M.G. Grimaldi, Phys. Status Solidi A **212**, 1662 (2015)
29. K. McCafferty, A. Soper, C. Cheung, J. Shirokoff, U. Erb, Scr. Metall. Mater. **26**, 1215 (1992)

Cite this article as: Ségolène Combettes, Teresa Hungria, Sophie Barre, Béatrice Pecassou, Robin Cours, Magali Benoit, Marie-José Casanove, Anne Ponchet, Patrizio Benzo, Self-organization mechanisms in a Fe-Au film: from isolated core-shell to multicore nanoparticles, Eur. Phys. J. Appl. Phys. **97**, 27 (2022)